Predicting High-Lift Low-Pressure Turbine Cascades Flow Using Transition-Sensitive Turbulence Closures

Roberto Pacciani
e-mail: roberto.pacciani@unifi.it

Michele Marconcini

Andrea Arnone

Department of Industrial Engineering
University of Florence
via di Santa Marta,
3 Firenze 50139, Italy

Francesco Bertini
Avio S.p.A. via I Maggio, 99,
Rivalta di Torino (TO) 10040, Italy

This paper discusses the application of different transition-sensitive turbulence closures to the prediction of low-Reynolds-number flows in high-lift cascades operating in low-pressure turbine (LPT) conditions. Different formulations of the well known $\gamma-\tilde{Re}_{\theta t}$ model are considered and compared to a recently developed transition model based on the laminar kinetic energy (LKE) concept. All those approaches have been coupled to the Wilcox $k-\omega$ turbulence model. The performance of the transition-sensitive closures has been assessed by analyzing three different high-lift cascades, recently tested experimentally in two European research projects (Unsteady Transition in Axial Turbomachines (UTAT) and Turbulence and Transition Modeling for Special Turbomachinery Applications (TATMo)). Such cascades (T106A, T106C, and T108) feature different loading distributions, different suction side diffusion factors, and they are characterized by suction side boundary layer separation when operated in steady inflow. Both steady and unsteady inflow conditions (induced by upstream passing wakes) have been studied. Particular attention has been devoted to the treatment of crucial boundary conditions like the freestream turbulence intensity and the turbulent length scale. A detailed comparison between measurements and computations, in terms of blade surface isentropic Mach number distributions and cascade lapse rates will be presented and discussed. Specific features of the computed wake-induced transition patterns will be discussed for selected Reynolds numbers. Finally, some guidelines concerning the computations of high-lift cascades for LPT applications using Reynolds-averaged Navier–Stokes (RANS)/unsteady RANS (URANS) approaches and transition-sensitive closures will be reported.
[DOI: 10.1115/1.4025224]

Introduction

The increasing demand for compact and light aircraft engines with high efficiency has led to the development of high-lift and ultrahigh-lift airfoils for the low-pressure (LP) turbine. Low-pressure turbine blades work with relatively low Reynolds numbers, and such flow conditions may be particularly critical for the suction side boundary layer, which is responsible for the greatest contribution to the profile loss (up to the 85%). On isolated blade rows, low Reynolds number operations are likely to produce boundary layer separation in regions of adverse pressure gradient, and an important loss penalty is associated with these circumstances. In the engine multistage environment, the unsteady wake-induced transition plays a key role in reducing the separation effects up to a level compatible with acceptably low losses. Several studies demonstrate how high-lift [1,2] and ultrahigh-lift [3–6] airfoils can be operated with loss control by taking advantage of wake-induced transition in LPT low-Reynolds-number flows.

The suction side boundary layer behavior is modulated by its interaction with the incoming wakes. The velocity deficit and the high turbulence energy within the wakes can induce transition. Such a mechanism can reduce of even prevent the boundary layer separation. Many studies [6–9] have shown how, after the wake passing, the boundary layer tends to relax to its pretransitional state. This determines a condition characterized by essentially laminar, but attached flow, referred to as *calming*. Once such an effect has decayed, if the wake passing frequency is not too high, the boundary layer begins to separate again. It is the relative influence of laminar, separated, turbulent, and calmed boundary layer portions that is responsible of the loss reduction with respect to steady inflow cases.

The flow features described above have significant implications for blade design. For example, with several cascade tests with and without incoming wakes, Coull et al. [10] have demonstrated how suitable loading distributions can reduce the penalty associated with low-Reynolds-number flows in high-lift bladings. Generally speaking, there is a strong industrial interest in tools that can help designers to exploit and improve the high-lift concept for the design of the next generation of aeroengines. Transition prediction methodologies represent a key requirement in this scenario. Albeit large eddy simulation or direct numerical simulation (DNS) approaches can be of great help in the physical understanding of the intimate structure of transition mechanisms, such methodologies are way far from being feasible from an engineering point of view. Consequently, despite an unavoidable lack of physical details, RANS/URANS approaches, accompanied with reliable transition models, are strongly desirable.

Today, in industrial computational fluid dynamics (CFD) approaches, the majority of the methodologies for modeling bypass or separated-flow transition are based on the intermittency concept (e.g., Suzen et al. [11] Menter et al. [12]). For example, Langtry and Menter [13] have coupled an intermittency and a transition-onset Reynolds number transport model to obtain a dynamic description of the transition, which makes use of local variables only. Such a model is conceived as a general framework to include correlation-based transition criteria in RANS/URANS solvers overcoming the difficulties associated with the use of

Contributed by the International Gas Turbine Institute (IGTI) of ASME for publication in the JOURNAL OF TURBOMACHINERY. Manuscript received June 13, 2013; final manuscript received July 29, 2013; published online September 27, 2013. Editor: Ronald Bunker.

nonlocal variables. Since the time of its introduction the Langtry and Menter model has become very popular, and many researchers have taken advantage of its flexibility in order to test their own correlations. The works of Content and Houdeville [14] and Suluksna et al. [15] are only some examples of transitional flow computations based on this methodology. The work of Babajee and Arts [16] represents a successful attempt to predict separated flow transition in high-lift cascades using the Langtry and Menter model.

Recently, the laminar kinetic energy (LKE) concept has also received considerable attention in the field of transition modeling. The LKE-based methodologies are characterized by conventional transport models that can readily be formulated in terms of local flow quantities. They are able to address the rise of pretransitional fluctuations in boundary layers and their subsequent breakdown to turbulence. Walters and Leylek [17,18] and Lardeau et al. [19] exploited the LKE concept, originally introduced by Mayle and Schulz [20], to sensitize a two-equation model to the onset of steady natural and bypass transition. Examples of successful applications of the LKE approach to LP turbines have been provided by Lardeau and Leschziner [21] and by Pacciani et al. [22]. In the latter case a novel formulation for the LKE transport equation was proposed in order to predict steady separated flow transition in high-lift cascade. However, the extension of LKE-based approaches, like the one proposed in Ref. [22], for the analysis of unsteady wake-induced transition is not straightforward. Transition is triggered via the energy transfer between the laminar fluctuation regime and the turbulence field and is accomplished by means of a suitable coupling between the LKE transport equation and the eddy-viscosity model. When periodic unsteady conditions are considered, such a coupling should guarantee that no laminar kinetic energy is created in the wake-induced path, transition being induced by the diffusion of wake turbulence into the boundary layer. It should instead be allowed to develop in the path between wakes in order to model the boundary layer instabilities and promote transition. Such a goal is achieved by introducing another transport equation for the so called *turbulence indicator function* [23]. Its role is to identify the fraction of time over which the boundary layer, at a given spatial location, is affected by the wake turbulence and it represents the desired mean for combining the pretransitional and turbulent components of the modelization.

The main purpose of this work is to assess the capabilities of the aforementioned methodologies to provide engineering predictions of steady and unsteady high-lift cascade flows at low Reynolds number. The LKE model was specifically conceived and tuned for separated flow transition. The $\gamma-\tilde{\mathrm{Re}}_{\theta t}$ model is a flexible and general framework suitable for predictions of transition occurring in either the natural, bypass, or separated flow mode. A comparison evidencing the relative merits of the two methodologies is then considered very interesting for industrial applications. Several formulations of the Langtry and Menter model, namely the original approach, the Content and Houdeville [14] and the Suluksna et al. [15] formulations were analyzed. All the transition prediction frameworks have been coupled with the Wilcox $k-\omega$ turbulence model.

Three high-lift cascades (T106A, T106C, and T108), recently tested at the von Kármán Institute and at the University of Cambridge, in the framework of the two European research projects, Unsteady Transition in Axial Turbomachines (UTAT) and Turbulence and Transition Modeling for Special Turbomachinery Applications (TATMo), were considered for the present study. The analyzed Reynolds number values span the whole range typically encountered in aeroengine low-pressure turbine operations. Steady and unsteady inflow conditions brought about by incoming wakes, with reduced frequencies representative of typical operations of modern LP turbines, have been studied. Detailed comparisons between measurements and computations in terms of blade surface isentropic Mach number distributions and cascade lapse rates will be presented and discussed. Specific features of the computed wake-induced transition patterns will also be discussed.

Computational Framework

The Flow Solver. The TRAF code (Arnone et al. [24]) was used in the present work. The unsteady, three-dimensional, Reynolds-averaged Navier–Stokes equations are written in conservative form in a curvilinear, body-fitted coordinate system and solved for density, absolute momentum components, and total energy. A dual-time-stepping method [25,26] is used to perform time accurate calculations.

The LKE-Based Transition/Turbulence Model. The proposed model is based on four transport equations for the laminar (k_ℓ) and turbulent (k) kinetic energies, the specific turbulent-dissipation rate (ω), and the turbulent indicator function (I), respectively:

$$\frac{Dk_\ell}{Dt} = (1-I)P_\ell - 2\nu\frac{k_\ell}{y^2} + \nu\nabla^2 k_\ell - R \tag{1}$$

$$\frac{Dk}{Dt} = IP_k - \beta^* f_k k\omega + \frac{\partial}{\partial x_j}\left[(\nu+\sigma_k\nu_T)\frac{\partial k}{\partial x_j}\right] + R \tag{2}$$

$$\frac{D\omega}{Dt} = \alpha I\frac{\omega}{k}P_k - \beta\omega^2 + \frac{\partial}{\partial x_j}\left[(\nu+\sigma_\omega\nu_T)\frac{\partial \omega}{\partial x_j}\right] \tag{3}$$

$$\frac{DI}{Dt} = P_I + \frac{\partial}{\partial x_j}\left[(\nu+\sigma_I\nu_T)\frac{\partial I}{\partial x_j}\right] \tag{4}$$

A detailed description of the model can be found in Ref. [23]. Here, for conciseness, only its most significant features will be discussed. The turbulent indicator function I is a key feature of the present modeling strategy. Physically it can be regarded as the probability that the flow, at a given spatial location, is turbulent, with $0 \le I \le 1$. Thus, $I=0$ refers to purely laminar flow, while $I=1$ indicates a turbulent regime (see Rumsey et al. [27]). The role of the turbulent indicator function is to weigh the production terms of the laminar fluctuations and turbulence energy so that they are activated depending on the turbulence level inside the boundary layer. Therefore, the production term for the I equation was assumed to be proportional to the turbulent Reynolds number, which gives a measure of the local turbulence intensity, and it was constructed as follows:

$$P_I = c_I\frac{U^2}{\nu}\left(\tilde{\mathrm{Re}}_T - I\right) \tag{5}$$

where: $\tilde{\mathrm{Re}}_T = (\mathrm{Re}_T - \mathrm{Re}_{T\infty})/\mathrm{Re}_{T\infty}$, and $\mathrm{Re}_{T\infty}$ is the freestream value of the turbulent Reynolds number. The term ν/U^2 represents a viscous time scale. Finally, the function I, as obtained by the integration of Eq. (4), is limited between 0 and 1.

With reference to periodic unsteady conditions, the turbulence indicator function can be regarded as a sensor that identifies the fraction of the period over which the boundary layer, at a given spatial location, is affected by wake turbulence. In this condition the generation of laminar fluctuating energy is suppressed and the wake-induced transition process is controlled by the diffusion of wake turbulence into the boundary layer. This transition mode is made possible via the low-Reynolds formulation of the turbulent transport Eqs. (2) and (3) (e.g., Wilcox [28]). In the path between wakes, the function I goes to very low values. This allows transition to be determined by the laminar kinetic energy growth in the boundary layer. It is worthwhile to notice how the turbulence indicator function is conceptually different from the intermittency factor, in the sense that it does not control the transition process but simply enables different transition modelizations in the wake passing period.

The LKE transport model is based on the laminar kinetic energy concept of Mayle and Schulz [20], which enables to take

into account the pretransitional rise of the fluctuating kinetic energy. In attached and separated shear layers, the amplification of fluctuations is due more to conventional shear-stress/strain interaction (Lardeau et al. [29]) rather than to pressure diffusion (Mayle and Schulz [20]). Hence, a model of the production of the laminar kinetic energy can be formulated as follows:

$$P_\ell = \nu_\ell S^2; \quad \nu_\ell = C_1 f_1(\mathrm{Tu}_\infty)\sqrt{k_\ell}\delta_\Omega \tag{6}$$

where $f_1(\mathrm{Tu}_\infty) = \max\{0.8, 2\tanh\sqrt{\mathrm{Tu}_\infty/4.5}\}$.

Once the laminar kinetic energy is created in the separated shear layer, it must be transferred to the turbulence field to trigger the transition process, as shown by numerical [30] and experimental investigations [31]. This is accomplished via the term R, which appears in both the laminar and turbulent kinetic energy equations, but with opposite signs, resulting in no net change of the total fluctuating kinetic energy $k_{\mathrm{tot}} = k_\ell + k$. Rather there is a transfer of energy from k_ℓ to k. Following Walters and Leylek [17], this term is assumed to be proportional to k_ℓ

$$R = C_2\beta^* f_2 \omega k_\ell \tag{7}$$

The damping function f_2 is defined as follows:

$$f_2 = 1 - e^{-\psi/C_3}; \quad \psi = \max(0, IR_y - C_4) \tag{8}$$

The quantity ψ can be considered as a transition parameter because it controls the transfer of energy from the laminar to the turbulent state, which occurs when the Reynolds number R_y, multiplied by the turbulent indicator function I, reaches the threshold value C_4.

The turbulence closure is derived from the Wilcox's low-Reynolds-number $k-\omega$ model [28]. The turbulence-production term is written as

$$P_k = \tau_{ij}\frac{\partial u_i}{\partial x_j} = \nu_T S^2; \quad \nu_T = f_\mu \frac{k}{\omega} \tag{9}$$

The terms $f_k(\mathrm{Re}_T)$ in Eq. (2) and $f_\mu(\mathrm{Re}_T)$ in Eq. (9) are closure functions. Their definitions are given in Ref. [23] together with the values of the various constants.

The inlet condition for the indicator function is

$$I = \min[(\mathrm{Re}_T - \mathrm{Re}_{T\infty})/\mathrm{Re}_{T\infty}, 1]$$

The boundary condition at a wall is zero normal gradient.

The inlet condition for the laminar kinetic energy is $k_\ell = 0$. The boundary condition at a wall is $k_\ell = 0$. The turbulence equations of the present model yield the correct asymptotic behavior at solid boundaries [28].

The $\gamma-\tilde{\mathrm{Re}}_{\theta t}$ Models. The model consists of two transport equations, one for the intermittency function (γ) and the other for the transition-onset momentum thickness Reynolds number ($\tilde{\mathrm{Re}}_{\theta t}$), namely

$$\frac{D\gamma}{Dt} = P_\gamma - E_\gamma + \frac{\partial}{\partial x_j}\left[\left(\nu + \frac{\nu_T}{\sigma_f}\right)\frac{\partial \gamma}{\partial x_j}\right] \tag{10}$$

$$\frac{D\tilde{\mathrm{Re}}_{\theta t}}{Dt} = P_{\theta t} - \frac{\partial}{\partial x_j}\left[\sigma_{\theta t}(\nu + \nu_T)\frac{\partial \tilde{\mathrm{Re}}_{\theta t}}{\partial x_j}\right] \tag{11}$$

The intermittency source terms are written as

$$P_\gamma = F_{\mathrm{length}} c_{a1} S(\gamma F_{\mathrm{onset}})^{0.5}(1 - c_{e1}\gamma); \quad E_\gamma = c_{a2}\Omega F_{\mathrm{turb}}(c_{e2}\gamma - 1) \tag{12}$$

while the one for the $\tilde{\mathrm{Re}}_{\theta t}$ equation is given by

$$P_{\theta t} = c_{\theta t}\frac{\mathrm{Re}_{\theta t} - \tilde{\mathrm{Re}}_{\theta t}}{t}(1 - F_{\theta t}); \quad t = \frac{500\nu}{U^2} \tag{13}$$

The complete definitions of closure functions and the values of the various constants can be found in Ref. [13]. For the sake of conciseness, in the present work only some fundamental aspects of the modelization will be discussed. The onset of transition is controlled by the function F_{onset}, which is based on the ratio $\mathrm{Re}_v/(2.193\mathrm{Re}_{\theta c})$ between the vorticity Reynolds number and a critical value of the momentum thickness Reynolds number. The transition region length is instead controlled by the function F_{length}. The model is conceived as general framework for implementing correlation-based transition criteria into general purposes flow solvers avoiding the use of nonlocal quantities. The correlations that must be provided to close the model are of the following form:

$$\mathrm{Re}_{\theta t} = f(\mathrm{Tu}, \lambda_\theta); \quad \mathrm{Re}_{\theta c} = f(\tilde{\mathrm{Re}}_{\theta t}); \quad F_{\mathrm{length}} = f(\tilde{\mathrm{Re}}_{\theta t}) \tag{14}$$

The quantity $\mathrm{Re}_{\theta t}$ represents a transition onset momentum thickness Reynolds number. Its expression as a function of the Thwaites parameter λ_θ and turbulence intensity Tu is given in Langtry and Menter [13]. Such a quantity is calculated locally at any point of the computational domain. The function

$$F_{\theta t} = \min\left[\max\left(F_{\mathrm{wake}} e^{-\left(\frac{y}{\delta}\right)^4}, 1 - \frac{\gamma - 1/c_{e2}}{1 - 1/c_{e2}}\right), 1\right] \tag{15}$$

with

$$F_{\mathrm{wake}} = e^{-\left(\frac{\mathrm{Re}_\omega}{10^5}\right)^2}; \quad \mathrm{Re}_\omega = \frac{\omega y^2}{\nu}; \quad \delta = 375\frac{\tilde{\mathrm{Re}}_{\theta t}\nu y\Omega}{U^2} \tag{16}$$

which appears in the source term of Eq. (11), is designed to be equal to 1 in the boundary layer and 0 in the freestream, where the source term $P_{\theta t}$ must be active in order to force the transported quantity $\tilde{\mathrm{Re}}_{\theta t}$ to be equal to the transition onset momentum thickness Reynolds number $\mathrm{Re}_{\theta t}$. In the boundary layer the source term $P_{\theta t}$ is nullified so that the value of $\tilde{\mathrm{Re}}_{\theta t}$ is controlled by diffusion from the freestream. Correlations for the critical momentum thickness Reynolds number $\mathrm{Re}_{\theta c}$ and the function F_{length} have been proposed by several authors. The ones that have been considered for the present work come from the contributions of Langtry and Menter [13], Content and Houdeville [14], and Suluksna et al. [15]. They reported successful computations of transitional flows over a wide range of applications. The corresponding set of correlations will be referred to as LM, CH, and SDJ models in the following. With respect to the original formulations no further tuning of the correlations was attempted in the present work.

In order to allow the prediction of realistic reattachment locations in separation-induced transition, Langtry and Menter [13] proposed a correction to the intermittency factor given by Eq. (10) by introducing a "separation aware" term of the form

$$\gamma_{\mathrm{sep}} = \min\left\{2\max\left[\frac{\mathrm{Re}_v}{3.235\mathrm{Re}_{\theta c}} - 1, 0\right]F_{\mathrm{reattach}}, 2\right\}F_{\theta t} \tag{17}$$

$F_{\mathrm{reattach}} = \exp[-(\mathrm{Re}_T/20)^4]$, and by defining an effective intermittency as

$$\gamma_{\mathrm{eff}} = \max(\gamma, \gamma_{\mathrm{sep}}) \tag{18}$$

which is finally used in the coupling with the turbulence model [13]. The role of Eqs. (17) and (18) is to allow the effective intermittency to raise above the unity in transitional separated flow

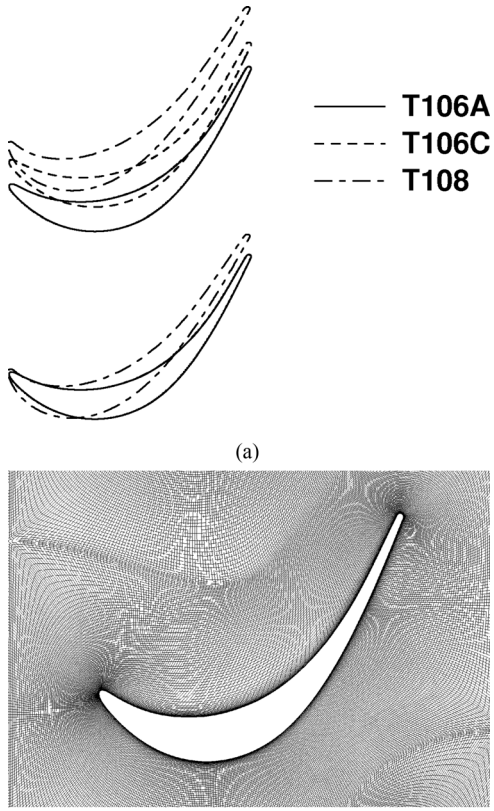

Fig. 1 (*a*) Analyzed cascades configurations, (*b*) T106C – single-block O-type grid 641×101

regions, thus enabling a rapid growth of the turbulent kinetic energy that promotes boundary layer reattachment. It is worthwhile to notice how the increase of γ_{sep} depends on the value of the critical Reynolds number $Re_{\theta c}$ in the separation. Then the turbulence production in the breakdown region of the bubble is strongly dependent on the $Re_{\theta c}$ distribution and so is for the reattachment location. The function F_{length} has a minor influence in separated flow transition.

When dealing with unsteady calculations with incoming wakes, an erratic behavior of the function $F_{\theta t}$ was sometimes detected. The problem was identified in the dependence of the function F_{wake} on the product Ωy, between the vorticity magnitude and the distance from the wall. In the presence of relevant vorticity spots occurring far from the walls (the case of incoming wakes) such a quantity can become very large. As a consequence the parameter δ becomes also very large and the function $F_{\theta t}$ switches to 1 outside the boundary layer, thus producing an unbalance of the $\tilde{Re}_{\theta t}$ equation. This prevents the boundary layer from being fed with the low values of $\tilde{Re}_{\theta t}$ that exist within the wake, thus suppressing wake-induced transition. In order to overcome this difficulty the dependence on the vorticity magnitude was eliminated from the function $F_{\theta t}$. This was achieved by simply redefining δ as

$$\delta = 170\frac{\tilde{Re}_{\theta t}\nu}{U} \tag{19}$$

Such a modification was found to have negligible effects on the predictions for steady transition.

The coupling of the $\gamma-\tilde{Re}_{\theta t}$ model with the Wilcox's $k-\omega$ turbulence model was carried out as in Ref. [13].

The Test Cases

Two of the test cases that were selected for the present study are based on the T106 blade section, while the third one is based on the T108 profile. The airfoil geometries and the different pitch/chord ratios of the three configurations can be appreciated in Fig. 1(*a*). The T106 turbine blade section [32] is a widely used geometry for both experimental and numerical studies on high-lift LP profiles. Detailed experimental data are available for a range of incidence, cascade solidity, and Reynolds number. Two different solidity values have been studied in the present paper, corresponding to the T106A and T106C cascades of Fig. 1(*a*). The T108 cascade is representative of a front loaded blade section and, with respect to T106C cascade, it shows a much gradual diffusion from the suction velocity peak to the blade trailing edge. At all the Reynolds numbers, separation bubbles occurring on the blade suction side were then expected to be smaller with respect to the T106C case.

Table 1 Main flow parameters for the cascades

	T106C	T106A	T108
α_1	32.7 deg	37.7 deg	35.5 deg
s/c	0.95	0.8	1.10
M_{2is}	0.65	0.04	0.65
$\ell_{T\infty}/c_x$	2.5×10^{-3}	1×10^{-3}	2.5×10^{-3}
Tu_∞	0.80%; 1.8%; 2.6%	4.0%	0.80%
f_r	0.70	0.68	0.53

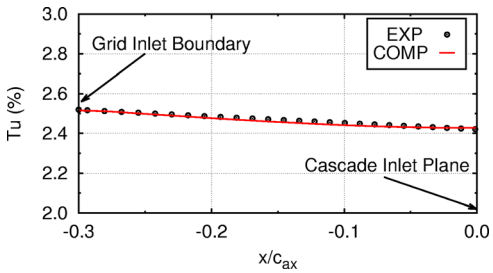

Fig. 2 Turbulence decay upstream of the T106C and T108 cascades ($Re_{2,is} = 1.6\times10^5$)

The main geometric and flow conditions for the analyzed configurations are summarized in Table 1. The T106C and the T108 cascades were tested at the von Kármán Institute during the UTAT and TATMo projects. Measurements were carried out in a high-speed facility conceived to reproduce the actual cruise operation of modern aeroengine LP turbines. A grid was positioned upstream of the cascade in order to produce different freestream turbulence levels. The axial distance between the grid and the blade leading edge was varied in order to prescribe the appropriate turbulence level at the cascade inlet plane. The turbulence decay upstream of the cascade was also characterized. An example of the computed turbulence level as a function of the distance from the cascade inlet section is compared to the measured one in Fig. 2. As reported in Table 1, the numerical results were obtained with a turbulent scale value of $\ell_T/c_{ax} = 2.5\times10^{-3}$, which is practically coincident with the one given by the mixing length formula: $\ell_{mix} = 0.18\times r_G$, when the grid rods radius r_G is assumed as a reference dimension. The test rig was equipped with a moving bar wake-generator that ensured a reduced frequency representative of actual rotor-stator interactions in cruise conditions. Detailed traverse measurements within the wakes were made available for code validation purposes. Steady measurements were carried out on a range of Reynolds number going from $Re_{2,is} = 0.8\times10^5$ to $Re_{2,is} = 1\times10^5$. Unsteady experimental results were made available only for low freestream turbulence intensity and two values of the Reynolds number corresponding to $Re_{2,is} = 1\times10^5$ and $Re_{2,is} = 1.4\times10^5$.

The T106A cascade was tested at the University of Cambridge in low-speed (incompressible) conditions. Steady and unsteady measurements were carried out on a range of flow conditions

similar to the one reported for the T106C and T108 cascades tests. In particular, very detailed boundary layer measurements were provided for selected flow conditions, and this makes such a configuration a very interesting one for the validation of time-accurate procedures.

A 641 × 101 O-type grid was used for all the calculations. The mesh size, which can be appreciated in Fig. 1(*b*), was selected in order to have sufficient grid density to prevent smearing of the incoming wakes [23]. About 40 cells lie inside laminar portions of boundary layers and the y^+ values of the mesh nodes closest to the wall are below unity in turbulent regions.

The T108 Turbine Cascade

For the T108 cascade, detailed numerical analyses were previously carried out using a three-equation $k_\ell - k - \omega$ model (Pacciani et al. [33]). Those results are virtually identical to the ones obtained with the present $I! - k_\ell - k - \omega$ model. Actually there is no point in employing the fourth equation for the turbulence indicator function in steady inflow calculations. It has been used in the present work only to discuss comparisons between homogeneous numerical results in steady and unsteady cases.

Figure 3 compares calculated and measured isentropic Mach number distributions along the blade suction side for three different values of the Reynolds number and for an inlet turbulence level of $Tu_\infty = 0.8\%$. For clarity, only the portion of the blade suction side that exhibited boundary layer separation is analyzed in Fig. 3. Sensible differences can be noticed between the predictions obtained with the various formulations of the $\gamma - \tilde{Re}_{\theta t}$ model. Such differences are comparable to the ones found with the LKE-based model results. The experimental distributions suggest that the suction side boundary layer is mildly separated at the highest Reynolds number and that the separated flow region has still the structure of a short bubble even at the lowest Reynolds number ($Re_{2,is} = 0.8 \times 10^5$). The maximum bubble thickness is somewhat underestimated by the LKE-based model, especially at the lowest Reynolds number (Fig. 3(*a*)), but the experimental transition location seems to be reasonably matched and so the separated flow region extent. Similar conclusions can be drawn for the CH model. Separation bubble sizes obtained with the other formulations of the $\gamma - \tilde{Re}_{\theta t}$ model are similar to the measured one only at the intermediate Reynolds number value (Fig. 3(*b*)). When the Reynolds number was varied in the range between $Re_{2,is} = 1.2 \times 10^5$ and $Re_{2,is} = 2 \times 10^5$ the separation bubble was found to have approximately the same extension in the LM and SDJ calculations, thus resulting in overestimation for the highest Reynolds numbers cases. For the lowest Reynolds number case, the results of Fig. 3(*a*) suggest that the boundary layer is not even reattached at the trailing edge in the LM and SDJ simulations. This is confirmed by the wall shear stress distributions along the blade suction side shown in Fig. 4. Experimental quasi-wall shear stress values are also reported for comparison. Depending on the Reynolds number the experimental separation point is located between $x/c_{ax} = 0.6$ and $x/c_{ax} = 0.65$, while the reattachment point lies between the 80% and the 90% of the suction side length. As suspected, at $Re_{2,is} = 0.8 \times 10^5$ only the LKE and CH models

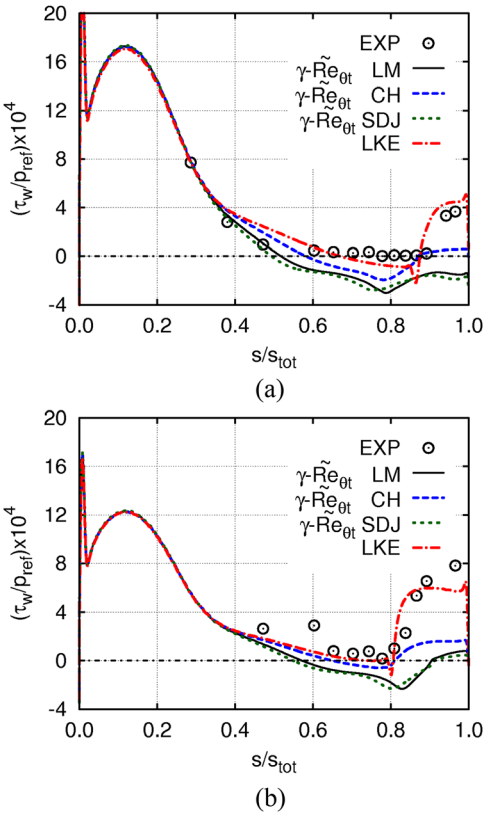

Fig. 4 T108 cascade: wall shear stress distributions (*a*) $Re_{2,is} = 0.8 \times 10^5$ (*b*) $Re_{2,is} = 2 \times 10^5$

predict boundary layer reattachment. Its location is in substantial agreement with the experimental one. Computations performed with the LM and SDJ models are characterized by an open separation that extends downstream the blade trailing edge. Also at the highest Reynolds number ($Re_{2,is} = 2 \times 10^5$) the separated flow region computed by these two models appears too large. A common feature of the various $\gamma - \tilde{Re}_{\theta t}$ models is the low value of the wall shear stress in the breakdown region of the bubble. On the contrary, measurements show a sudden increase in the quasi-wall shear-stress distribution downstream the reattachment location. In this region the LKE-based model shows a more realistic behavior, which is determined by the energy transfer term R of Eq. (7).

The observations concerning the computed separation bubble extent and the wall shear-stress distributions are consistent with the results of Fig. 5, which compares predicted and measured kinetic energy loss coefficients as a function of the Reynolds number. The high losses in the LM and SDJ calculations are associated with the open separations predicted by those models. Also the LKE-based model tends to slightly overestimate the cascade kinetic energy loss coefficient, but the agreement with experiment is satisfactory. The CH model results agree quite well

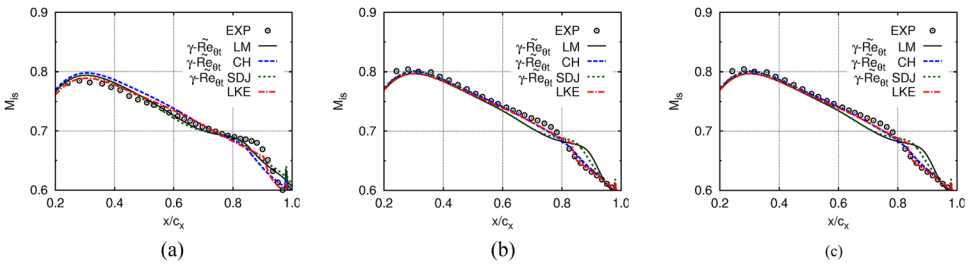

Fig. 3 T108 cascade: experimental [16] and computed isentropic Mach number distributions along the blade suction side (*a*) $Re_{2,is} = 0.8 \times 10^5$ (*b*) $Re_{2,is} = 1.4 \times 10^5$ (*c*) $Re_{2,is} = 2 \times 10^5$

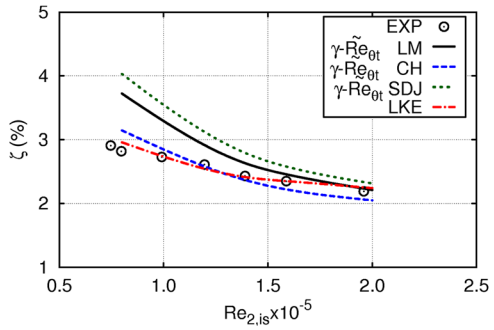

Fig. 5 T108 cascade: experimental [16] and computed Reynolds number lapse rate

with experiments but with a different trend in the Reynolds number lapse. CH model predictions are characterized by the formation of short bubbles at high Reynolds number. In this case major contributions to the total loss come from the turbulent stresses in the breakdown region. As noted before, the turbulent kinetic energy production with $\gamma-\tilde{\mathrm{Re}}_{\theta t}$ models tends to be lagged downstream the transition point and this leads to the underestimation of losses that can be noticed between $\mathrm{Re}_{2,\mathrm{is}} = 1.2 \times 10^5$ and $\mathrm{Re}_{2,\mathrm{is}} = 2 \times 10^5$. At low Reynolds number ($\mathrm{Re}_{2,\mathrm{is}} \leq 1.2 \times 10^5$) such a behavior can delay or even prevent the reattachment. Consequently, the separated flow region becomes a long bubble and losses become large and tend to follow a "laminar trend," thus rapidly increasing as the Reynolds number decreases. The results obtained with the CH model are in line with the calculations of Babajee and Arts [16] that were carried out with the same formulation.

The T106C Turbine Cascade

For the T106C cascade, steady and unsteady analyses were carried out in a range of Reynolds number and freestream turbulence intensities. The discussion will be split into two subsections concerning steady and time-accurate results.

Steady Results. Isentropic Mach number distributions on the blade suction side, for three different values of the Reynolds number, are compared to experiments in Fig. 6. The freestream turbulence level at the cascade inlet plane is $\mathrm{Tu}_\infty = 0.8\%$. In the range between $\mathrm{Re}_{2,\mathrm{is}} = 2.5 \times 10^5$ and $\mathrm{Re}_{2,\mathrm{is}} = 1.2 \times 10^5$, the separated flow region appears to have the structure of a short bubble (Figs. 6(*b*) and 6(*c*)) and such a flow feature is well reproduced by all the calculation, i.e., the effect of the flow separation on the calculated blade loading distribution is in good agreement with experiments. Consistently with what observed for the T108 cascade, the CH model predicts a slightly smaller separation bubble, while the LM and the SDJ formulations, together with the LKE-based model, yield the best results in these cases. Actually flow

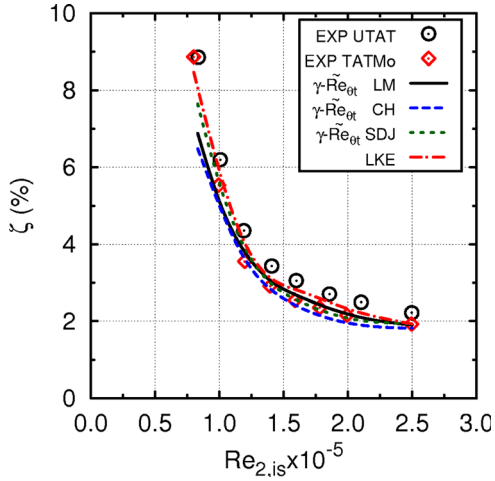

Fig. 7 T106C cascade: experimental [34] and computed Reynolds number lapse ($\mathrm{Tu}_\infty = 0.8\%$)

reattachment was experienced in all the $\gamma-\tilde{\mathrm{Re}}_{\theta t}$ simulations, as it can be deduced from the sharp pressure recovery downstream the maximum bubble thickness locations (Fig. 6). This circumstance is expected to be the result of the response of Eq. (17) to the stronger adverse pressure gradient experienced for this blade section with respect to the T108 cascade.

The spread between predictions of the $\gamma-\tilde{\mathrm{Re}}_{\theta t}$ models tends to increase when decreasing the Reynolds number. For $\mathrm{Re}_{2,\mathrm{is}} \leq 1.2 \times 10^5$ the separated flow region falls in the domain of the long bubbles and indeed an open separation is experienced for $\mathrm{Re}_{2,\mathrm{is}} = 0.8 \times 10^5$ [34]. In this case the LKE-based model yields the best results in capturing the deep modification occurring to the blade loading distribution, but the predictions of the $\gamma-\tilde{\mathrm{Re}}_{\theta t}$ models are nonetheless satisfactory.

Figure 7 compares computed and measured kinetic energy loss coefficients as a function of the Reynolds number. Two sets of measured data are included for comparison. They originate from different test performed within the European research projects UTAT and TATMo. For $\mathrm{Re}_{2,\mathrm{is}} \geq 1.2 \times 10^5$ the agreement is generally quite good except for a slight underestimation of losses by the CH and SDJ models. For lower values of the Reynolds number the relative differences between the predictions of the various methods and the discrepancy with experimental data become more pronounced, with computed loss coefficient values that are below the measured ones. The maximum spread of the results is recorded for the lowest Reynolds number. In fact, in the long bubble regime, small differences in the size of the computed separation reflect in sensible changes of the cascade loss. The very good performance of the LKE-based model at the lower Reynolds number stresses the fact that an accurate match of the separation effects on the blade loading distribution (Fig. 6(*a*)) usually results in a reliable prediction of losses. It must, however, be noted how

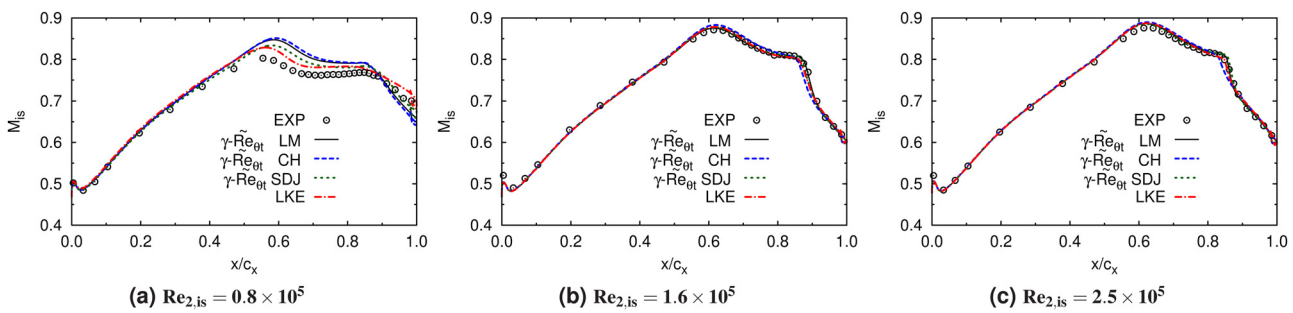

Fig. 6 T106C cascade: experimental [34] and computed isentropic Mach number distributions along the blade suction side ($Tu_\infty = 0.8\%$) (*a*) $\mathrm{Re}_{2,\mathrm{is}} = 0.8\times10^5$ (*b*) $\mathrm{Re}_{2,\mathrm{is}} = 1.6\times10^5$ (*c*) $\mathrm{Re}_{2,\mathrm{is}} = 2.5\times10^5$

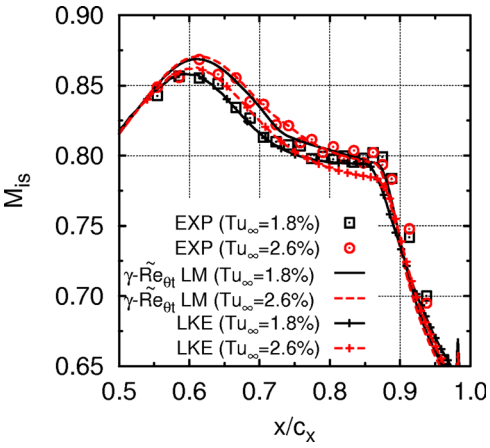

Fig. 8 T106C cascade: experimental [34] and computed isentropic Mach number distributions for different freestream turbulence levels ($Re_{2,is} = 0.8\times10^5$)

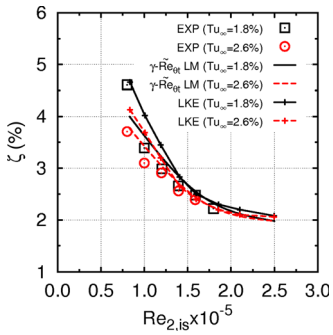

Fig. 9 T106C cascade: experimental [34] and computed cascade lapse rates for different freestream turbulence levels

the slope increase in the Reynolds lapse, which is associated with the bubble bursting phenomenon, is actually detected by all the numerical approaches. Such a change in slope can in fact be appreciated in both experiments and calculations at about $Re_{2,is} = 1.2 \times 10^5$ in Fig. 7. This is a remarkable aspect of the considered models as the reproduction of the correct trend in the Reynolds number lapse rate is very important for engineering simulations to be exploited for design purposes.

A freestream turbulence increase results in a reduction of the extension of the separated flow region [34]. For the T106C cascade, the most pronounced effects are recorded for the lower Reynolds numbers. The isentropic Mach number distributions, obtained with two different freestream turbulence intensities at the cascade inlet section ($Tu_\infty = 1.8\%$, and $Tu_\infty = 2.6\%$), are reported for the case with $Re_{2,is} = 0.8 \times 10^5$ in Fig. 8. For clarity, only the portion of the blade suction side of interest with respect to flow separation is shown. Increasing the freestream turbulence level from $Tu_\infty = 0.8\%$ to $Tu_\infty = 1.8\%$ results in a strong contraction of the separated flow region. As it can be deduced by the comparison between Fig. 6(*a*) and Fig. 8, the open separation that exists for $Tu_\infty = 0.8\%$ becomes a long bubble at higher freestream turbulence intensities. A strong pressure recovery associated with flow reattachment can in fact be observed in the last 15% of the blade axial chord. A further increase in the freestream turbulence intensity only results in a much weaker effect on the separated flow region, with small reductions of its extension and no appreciable change in structure. In terms of blade loading distributions, the changes in the separated flow configuration associated with the freestream turbulence increase are well reproduced in the calculations (Fig. 8). As far as $\gamma-\tilde{Re}_{\theta t}$ models are concerned, only the LM computations are reported, the other formulations giving very similar results. Both the models tend to underestimate the impact of the freestream turbulence increase from $Tu_\infty = 1.8\%$ to $Tu_\infty = 2.6\%$.

In particular, the LM model shows a very small variation in the blade loading distribution in this range of turbulence intensities. As shown by the comparison between Figs. 7 and 9, which reports Reynolds number lapse rates for $Tu_\infty = 1.8\%$ and $Tu_\infty = 2.6\%$, a strong reduction of the kinetic energy loss coefficient occurs for $Re_{2,is} < 1.2 \times 10^5$ when increasing the turbulence intensity from $Tu_\infty = 0.8\%$ to $Tu_\infty = 1.8\%$. Such a circumstance is associated with the contraction of the separation bubble size and it is well reproduced by computations also in terms of cascade loss. A sensible increase in the experimental lapse rate can still be observed for $Tu_\infty = 1.8\%$ when the Reynolds number is decreased below $Re_{2,is} < 1.2 \times 10^5$ and such a feature of the $Re_{2,is}-\zeta$ curve is correctly reproduced only by the LKE-based model, with an underestimation of the kinetic energy loss coefficient by the $\gamma-\tilde{Re}_{\theta t}$ model at low Reynolds numbers. For higher Reynolds numbers, predictions agree well with measurements for all the considered modelizations.

Unsteady Results. Time-resolved measurements of flow and turbulence quantities within the incoming wakes were taken during the experimental tests. Like in Pacciani et al. [23], they were used to prescribe time-dependent boundary conditions for the unsteady calculations. Unsteady experimental data were available for two different values of the Reynolds number corresponding to $Re_{2,is} = 1.4 \times 10^5$ and $Re_{2,is} = 1 \times 10^5$, respectively. Steady and unsteady computed isentropic Mach number distributions are compared to experiments in Figs. 10(*a*) and 10(*b*). Again, the various formulations of the $\gamma-\tilde{Re}_{\theta t}$ models yielded very similar predictions, so only the ones obtained with the LM model are reported. In terms of time-averaged blade loading distributions, the agreement can be considered very good along the whole suction side for both the considered Reynolds numbers. Computations performed with the LM- and LKE-based models gave practically coincident results. The effect of the separation bubble is almost suppressed by the interaction with the incoming wakes for the case at $Re_{2,is} = 1.4 \times 10^5$, and greatly reduced for $Re_{2,is} = 1 \times 10^5$. The load reduction in the front part of the blade with respect to steady conditions is also worth noting. It is caused by the decrease in incidence associated with the flow angle distribution within the wake.

For the T106C cascade, interaction between the boundary layer and the incoming wakes results in relevant cascade loss reductions with respect to steady inflow conditions. This is well evident from Fig. 10(*c*), which compares computed and measured cascade lapse rates, in terms of kinetic energy loss coefficient, with and without incoming wakes. The comparison between computed and measured values of the unsteady loss is also reported in Table 2 for the sake of clarity. Like for the isentropic Mach number distributions of Figs. 10(*a*) and 10(*b*) the agreement is very good. This suggests that the major effects of wake-induced transition are reproduced by both the LKE-based and $\gamma-\tilde{Re}_{\theta t}$ models.

Time-accurate calculations have been carried out in the range of Reynolds numbers between $Re_{2,is} = 1 \times 10^5$ and $Re_{2,is} = 2.5 \times 10^5$. In such a range the computed cascade lapse rate lies always below the steady one. Although the experimental data are not sufficient to confirm this trend, the same behavior was evidenced experimentally by Himmel and Hodson [35] in low-speed tests on the T106C cascade.

As mentioned in the Computational Framework section, the role of the turbulence indicator function I in the LKE-based model is to prevent the generation of the laminar fluctuations energy in the wake-induced path. This allows transition to be controlled by the diffusion of wake turbulence into the boundary layer. A convenient way to analyze this mechanism is based on distance-time diagrams of turbulence quantities. Examples of distance-time diagrams for the suction side of the T106C cascade are then reported for $Re_{2,is} = 1.4 \times 10^5$ in Fig. 11. They refer to the turbulence

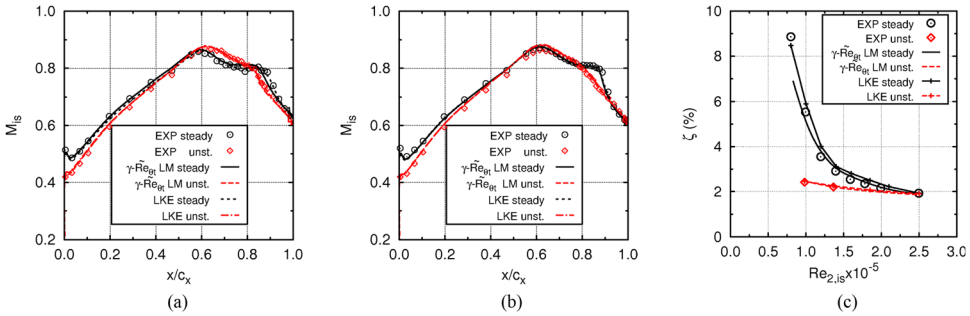

Fig. 10 T106C cascade: steady and unsteady isentropic Mach number distributions (*a*) $Re_{2,is} = 1\times10^5$, (*b*) $Re_{2,is} = 1.4\times10^5$, and (*c*) steady and unsteady cascade lapse rates

Table 2 T106C cascade: time-averaged kinetic energy loss coefficient for different Reynolds numbers and transition/turbulence models

$Re_{2,is} \times 10^5$	$\zeta(\%)$ Exp.	$\zeta(\%)$ LKE	$\zeta(\%)\ \gamma-\tilde{Re}_{\theta t}$ LM
1.4	2.20	2.25	2.21
1.0	2.42	2.45	2.46

indicator function I (Fig. 11(*a*)) and the average laminar kinetic energy within the suction side boundary layer (Fig. 11(*b*)). The distance from the leading edge is represented by the normalized curvilinear abscissa along the blade surface, while the time is nondimensionalized by the wake passing period. Two wake passing events are reported. Indeed in the wake-induced path the function I rapidly reaches its maximum value of 1 as a result of the diffusion of wake turbulence into the boundary layer (Fig. 11(*a*)). This condition implies the nullification of the laminar kinetic energy production term in Eq. (1). In the path between wakes the I function has a very low value and the laminar kinetic energy is left free to develop and promote transition (Fig. 11(*b*)).

The T106A Turbine Cascade

A complete set of experimental data was provided for a Reynolds number of $Re_{2,is} = 1.6 \times 10^5$ and an inlet turbulence level of $Tu_\infty = 4.0\%$. Unfortunately, the Tu decay rate downstream the turbulence generating device was not provided. Such information is of crucial importance to set up proper boundary conditions if faithful transition predictions are of primary importance [16]. In order to overcome this difficulty, it was decided to search for a turbulent length scale value that would guarantee a good match with measured cascade data in the steady case. Precursor calculations were carried out with the LKE-based model where the order of magnitude of the turbulent length scale was assumed equal to the one of the T108/T106C cases, but its value was varied until a good agreement with the experimental pressure coefficient was achieved on the blade suction side. A turbulent length scale value corresponding to $\ell_T/c_{ax} = 1 \times 10^{-3}$ was found to fulfill such requirements, and it was considered a realistic one. Results are compared to measurements in Fig. 12(*a*), in terms of pressure coefficient distribution and in Fig. 12(*b*), in terms of boundary layer shape factor. Boundary layer separation was detected on the blade suction side between 75% and 85% of the suction side length. To appreciate its effects on the pressure coefficient distribution, an enlargement of the last 40% of the suction side length is provided in Fig. 12(*a*). With respect to the T106C cascade, the suction side separation bubble is much smaller. This is due to the lower pitch/chord ratio that characterizes this configuration, which is located at the lower boundary of the high-lift domain. With the same boundary conditions setup, none of the $\gamma-\tilde{Re}_{\theta t}$ models predicts boundary layer separation, transition being of bypass type

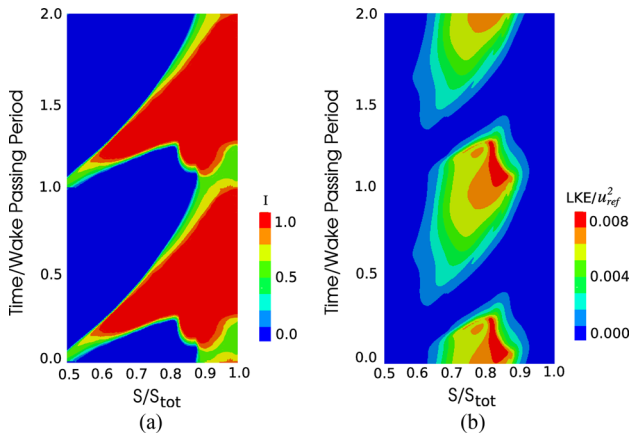

Fig. 11 T106C cascade: space time diagrams (*a*) turbulence indicator function (*b*) laminar kinetic energy, $Re_{2,is} = 1.4\times10^5$, $Tu_\infty = 0.8\%$

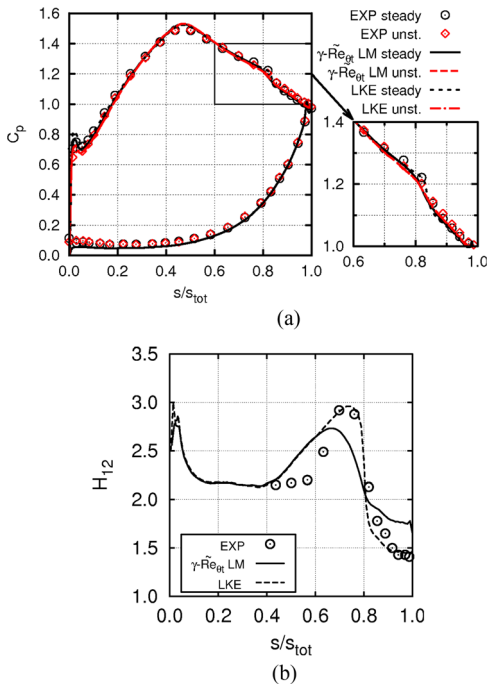

Fig. 12 T106A cascade: (*a*) experimental [6] and computed steady and unsteady pressure coefficient distributions, (*b*) steady boundary layer shape factor, ($Re_{2,is} = 1\times10^5$, $Tu_\infty = 4.0\%$)

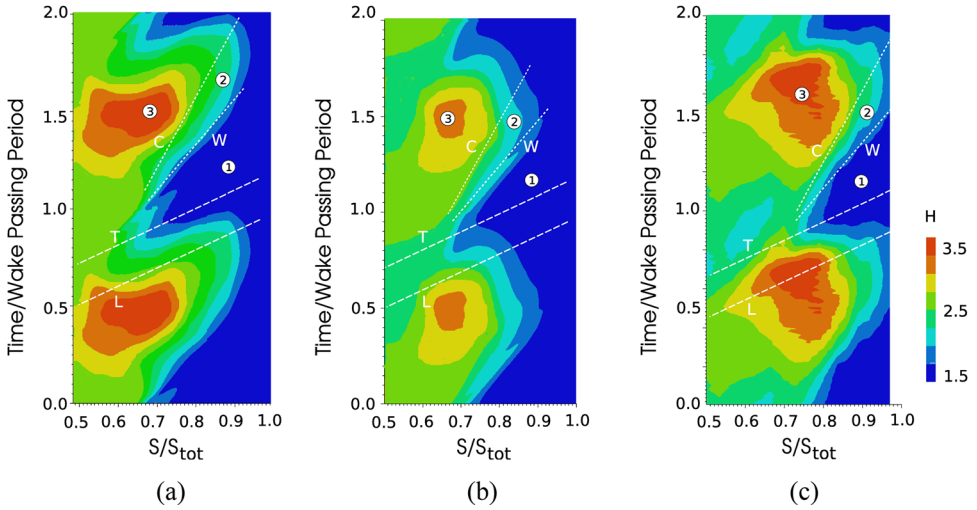

Fig. 13 T106A cascade: space time diagrams boundary layer shape factor (*a*) LKE-based model (*b*) $\gamma-\tilde{\mathrm{Re}}_{\theta t}$ LM model, (*c*) measured [6]

and starting very close to the separation point of the LKE-based calculation. Such a circumstance is quite evident both in terms of blade loading distribution (Fig. 12(*a*)) and boundary layer shape factor (Fig. 12(*b*)). Again, only the LM model results are reported, predictions with the other formulation being very similar and following the already discussed trends.

In order to establish proper boundary conditions for the unsteady calculations, the incoming wakes were modeled according to the procedure proposed by Lodefier and Dick [36]. The computed unsteady pressure coefficients are shown in Fig. 12(*b*), and they agree well with experimental data. The small suction side separation bubble that exists in steady inflow conditions practically disappears under the effect of the passing wakes. Time-averaged pressure coefficient distributions agree quite well with experiments for all the considered models. The time evolution of the boundary layer shape factor gives a comprehensive picture of the boundary layer state during the wake passing period. For the sake of conciseness, the comparison between computed and experimental unsteady results will be reported only in terms of this quantity in the form of the time-distance diagrams of Fig. 13. Regions characterized by low values of the shape factor ($H_{12} \simeq 1.4$) are representative of turbulent flow, while high values of this parameter ($H_{12} \simeq 3.5-4.0$) are associated with a separated, or nearly separated, laminar boundary layer. Trajectories L, T, C, and W were deduced from the measurements, and their meaning will be explained in the following. Lines L and T represent the loci of the wake leading and trailing edges in the free-stream. The wedge-shaped region of turbulent flow that can be identified between the T and W lines (marked as ① in the distance-time diagrams), is the result of wake-induced transition [6]. The high level of turbulence characterizing region ① is gradually reduced as the boundary layer tends to relax to its pretransitional state. The result of this process is the formation of the region ②, between the lines W and C, which is characterized by essentially laminar and attached flow, i.e., the calmed region. The computed wake-induced transition pattern closely resembles the experimental one, indicating that the major features of the boundary layer unsteady evolutions are captured by the analyzed methods. However, it can be noticed how in the calculations, wake-induced transition tends to begin at an upstream location with respect to experiments. This is particularly evident in the LKE-based prediction. More noticeable difference between computed unsteady results and experiments can be detected in the path between wakes. Here, the presence of a high shape factor region (marked as ③ in the space-time diagrams), both in the experiments and LKE-based calculation, indicates the reestablishment of flow separation. Such high values of H_{12} are not seen in the $\gamma-\tilde{\mathrm{Re}}_{\theta t}$ prediction. Moreover, transition is predicted earlier, in the path between wakes, with respect to both the LKE-based calculation and experiments. This is related to the occurrence of earlier transition experienced in steady calculations with the $\gamma-\tilde{\mathrm{Re}}_{\theta t}$ models.

Guidelines for the Study of High-Lift Cascades With Transition-Sensitive Turbulence Closures

Boundary conditions for turbulence quantities must be carefully set up on the basis of the available information concerning the test rig and experimental condition. This is true for all the considered models and it was found to be a very important step in order to perform meaningful comparisons between calculations and cascade measurements. In the authors' experience, the freestream turbulence level at the cascade inlet is generally known, while a complete characterization of the turbulence decay upstream of the test section may not be available. For the latter case, a reasonable estimation of the inlet turbulent length scale can be obtained by using the mixing length formula based on the radius r_G of the rods of the turbulence generating grid: $\ell_{\mathrm{mix}} = 0.18 \times r_G$. Otherwise, for validation purposes, one can select a turbulent length scale value that results in a comparable behavior of the boundary layer between numerical and experimental conditions. The achievement of such a goal can be evaluated by comparing the computed and measured effects of the separation on the blade loading distribution. For example, this allows the comparison of calculated and experimental cascade losses on a consistent basis. The above considerations have implications for design activities too. To this purpose, the numerical analysis of newly designed airfoils should be based on boundary conditions that are representative of the experimental setup where the airfoils will be eventually tested.

With reference to the $\gamma-\tilde{\mathrm{Re}}_{\theta t}$ model, care must be taken in the selection of the correlations (14) for the study of separated transitional flows. The correlations (14) have been defined to work together in order to yield the correct transition location and length (i.e., Refs. [13–15].). This typically happens in bypass transition cases, where the various formulations give very similar results. In separated flow, the critical Reynolds number $\mathrm{Re}_{\theta c}$ determines the value of γ_{sep} and then the turbulence production in the breakdown region of the bubble, while the companion F_{length} correlation plays a minor role. Consequently, different correlations for the critical Reynolds number can give very different results.

Concluding Remarks

Different transition models have been applied to the prediction of low Reynolds number flows in high-lift cascades operating in LP turbine conditions. They include a recently developed model based on the laminar kinetic energy concept and the Langtry and Menter $\gamma-\tilde{\mathrm{Re}}_{\theta t}$ model, completed with correlations by several researchers. The performance of the models was assessed by computing steady inflow cases as well as unsteady ones induced by incoming wakes.

Satisfactory results were obtained, in terms of blade surface isentropic Mach distributions and Reynolds number lapse in steady calculations of the T108 cascade with the LKE-based model. Results obtained with the $\gamma-\tilde{\mathrm{Re}}_{\theta t}$ model were found to be strongly dependent on the selected correlation for the critical Reynolds number. The LM and SDJ formulations gave separation bubble size systematically larger than the experimental ones and this implies the overestimation of losses. This was found to be related to an insufficient production of turbulent kinetic energy in the breakdown region of the bubble, which tends to delay the flow reattachment even if the transition location is correctly predicted.

Computed steady results for the T106C cascade were found to agree quite well with experiments for all the considered models in the short bubble regime. Nonetheless, the $\gamma-\tilde{\mathrm{Re}}_{\theta t}$ model performance is to be considered more or less case dependent, and this circumstance calls for an improvement of the separated flow transition component. Both the analyzed computational frameworks must be improved especially in the very low Reynolds number regime where the separated flow region configuration is very sensitive to variation in the Reynolds number itself or in the freestream turbulence level.

Time-accurate calculations revealed a very promising behavior of the considered models in the simulation of wake-induced transition for both the T106C and T106A cascade. Differences with time-resolved experimental data were evidenced, but the major features of such a complex phenomenon were reproduced by the calculations.

It is believed that the assessment carried out in the present work evidences, from an engineering point of view, the usefulness of the considered models for the design and analysis of high-lift profiles for aeroengine LP turbines.

Acknowledgment

The research reported in this paper was undertaken within the European Commission research project TATMo (Contract No. AST5-CT-2006-030939, www.tatmo.eu). Part of the experimental data were obtained within the research project UTAT (Contract No. G4RD-CT-2001-00628) funded by the European Commission. We would like to thank our fellow partners in European Union FP6 program TATMo for permitting the publication of our results in this paper.

Nomenclature

c = blade chord
C_p = pressure coefficient
f_r = reduced frequency, $f_r = u_{\mathrm{bar}} c/(s_{\mathrm{bar}} u_{2,\mathrm{is}})$
H_{12} = boundary layer shape factor, $H_{12} = \delta^*/\theta$
I = turbulence indicator function
k = turbulent kinetic energy
k_ℓ = laminar kinetic energy
ℓ_T = turbulence length scale, $\ell_T = k^{1/2}/\omega$
M = Mach number
R = transfer term
R_y = wall-normal-distance Reynolds number, $\sqrt{k}y/\nu$
Re_{is} = isentropic Reynolds number, $u_{is}c/\nu$
Re_T = turbulent Reynolds number, $k/(\nu\omega)$
Re_θ = momentum thickness Reynolds number, $u\theta/\nu$
$\tilde{\mathrm{Re}}_{\theta t}$ = local transition onset momentum thickness Reynolds number (transported quantity)
Re_v = vorticity Reynolds number, Sy^2/ν
s = blade pitch, curvilinear abscissa
S = mean shear rate $S = \sqrt{2S_{ij}S_{ij}}$
T = wake passing period
Tu = turbulence intensity, $\mathrm{Tu} = \sqrt{(2/3)k}/u$
u = velocity magnitude
x, y = Cartesian coordinates

Greek Symbols

α = flow angle
γ = intermittency
δ^* = boundary layer displacement thickness
δ_Ω = shear layer vorticity thickness, $\delta_\Omega = (u_\infty/2)(\partial u/\partial y)^{-1}_{\max_y}$
ζ = kinetic energy loss coefficient
θ = boundary layer momentum thickness
λ_θ = Thwaites pressure gradient parameter, $\lambda_\theta = (\theta^2/\nu)(du/ds)$
ν = kinematic fluid viscosity
τ_{ij} = Reynolds stress tensor
τ_w = wall shear stress
ω = specific turbulence-dissipation rate
Ω = vorticity magnitude

Subscripts

bar = relative to the moving bar wake generator
c = critical value
is = isentropic
ℓ = laminar
ref = reference value
t = transition onset
T = turbulent
1 = inflow
2 = outflow
∞ = freestream

Acronyms

CFD = computational fluid dynamics
CH = Content and Houdeville model
DNS = direct numerical simulation
HL = high-lift
KH = Kelvin–Helmholtz
LKE = laminar kinetic energy
LM = langtry and menter model
LPT = low-pressure turbine
SDJ = Suluksna, Dechaumphai, and Juntasaro model
TATMo = turbulence and transition modeling for special turbomachinery applications
URANS = unsteady Reynolds-averaged Navier–Stokes
UTAT = unsteady transition in axial turbines

References

[1] Cobley, K., Coleman, N., Siden, G., and Arndt, N., 1997, "Design of New Three Stage Low Pressure Turbine for the BMW Rolls-Royce BR715 Turbofan Engine," ASME Paper No. 97–GT–419.
[2] Curtis, E. M., Hodson, H. P., Banieghbal, M. R., Denton, J. D., Howell, R. J., and Harvey, N. W., 1997, "Development of Blade Profiles for Low Pressure Turbine Applications," ASME J. Turbomach., **119**(3), pp. 531–538.
[3] Haselbach, F., Schiffer, H. P., Horsman, M., Dressen, S., Harvey, N. W., and Read, S., 2002, "The Application of Ultra High Lift Blading in the BR715 LP Turbine," ASME J. Turbomach., **124**(1), pp. 45–51.
[4] Howell, R. J., Hodson, H. P., Schulte, V., Stieger, R. D., Schiffer, H. P., Haselbach, F., and Harvey, N. W., 2002, "Boundary Layer Development in the BR710 and BR715 LP Turbines—The Implementation of High–Lift and Ultra–High–Lift Concepts," ASME J. Turbomach., **124**(3), pp. 385–392.
[5] Schulte, V., and Hodson, H. P., 1998, "Unsteady Wake–Induced Boundary Layer Transition in High Lift LP Turbines," ASME J. Turbomach., **120**(1), pp. 28–35.

[6] Stieger, R. D., and Hodson, H. P., 2004, "The Transition Mechanism of Highly Loaded Low-Pressure Turbine Blades," ASME J. Turbomach., **126**(4), pp. 536–543.
[7] Banieghbal, M. R., Curtis, E. M., Denton, J. D., Hodson, H. P., Huntsman, I., Schulte, V., Harvey, N. W., and Steele, A. B., 1995, "Wake Passing in LP Turbine Blades," AGARD Conference, Derby, UK, May 8–12.
[8] Uzol, O., Zhang, X. F., Cranstone, A., and Hodson, H. P., 2007, "Investigation of Unsteady Wake-Separated Boundary Layer Interaction Using Particle-Image-Velocimetry," ASME Paper No. GT2007-28099.
[9] Satta, F., Simoni, D., Ubaldi, M., Zunino, P., and Bertini, F., 2010, "Experimental Investigation of Separation and Transition Processes on a High-Lift Low-Pressure Turbine Profile Under Steady and Unsteady Inflow at Low Reynolds Number," J. Therm. Sci., **19**(1), pp. 26–33.
[10] Coull, J. D., Thomas, R. L., and Hodson, H. P., 2010, "Velocity Distributions for Low Pressure Turbines," ASME J. Turbomach., **132**(4), p. 041006.
[11] Suzen, Y. B., Huang, P. G., Ashpis, D. E., Volino, R. J., Corke, T. C., Thomas, F. O., Huang, J., Lake, J. P., and King, P. I., 2007, "A Computational Fluid Dynamics Study of Transitional Flows in Low-Pressure Turbines Under a Wide Range of Operating Conditions," ASME J. Turbomach., **129**(3), pp. 527–541.
[12] Menter, F. R., Langtry, R. B., Likki, S. R., Suzen, Y. B., Huang, P. G., and Völker, S., 2006, "A Correlation-Based Transition Model Using Local Variables—Part I: Model Formulation," ASME J. Turbomach., **128**(3), pp. 413–422.
[13] Langtry, R. B., and Menter, F. R., 2009, "Correlation-Based Transition Modeling for Unstructured Parallelized Computational Fluid Dynamics Codes," AIAA J., **47**(12), pp. 2894–2906.
[14] Content, C., and Houdeville, R., 2010, "Local Correlation-Based Transition Model," 8th International ERCOFTAC Symposium on Engineering Turbulence Modelling and Measurements, Marseille, France, June 9–11, pp. 522–527.
[15] Suluksna, K., Dechaumphai, P., and Juntasaro, E., 2009, "Correlations for Modeling Transitional Boundary Layers Under Influences of Freestream Turbulence and Pressure Gradient," Int. J. Heat Fluid Flow, **30**, pp. 66–75.
[16] Babajee, J., and Arts, T., 2012, "Investigation of the Laminar Separation-Induced Transition With the $\gamma-\tilde{R}e_{\theta t}$ Transition Model on Low-Pressure Turbine Rotor Blades at Steady Conditions," ASME Paper No. GT2012-68687.
[17] Walters, D. K., and Leylek, J. H., 2004, "A New Model for Boundary Layer Transition Using a Single-Point RANS Approach," ASME J. Turbomach., **126**(1), pp. 193–202.
[18] Walters, D. K., and Leylek, J. H., 2005, "Computational Fluid Dynamics Study of Wake-Induced Transition on a Compressor-Like Flat Plate," ASME J. Turbomach., **127**(1), pp. 52–63.
[19] Lardeau, S., Leschziner, M. A., and Li, N., 2004, "Modelling Bypass Transition With Low-Reynolds-Number Nonlinear Eddy-Viscosity Closure," Flow Turbul. Combust., **73**, pp. 49–76.
[20] Mayle, R. E., and Schultz, A., 1997, "The Path to Predicting Bypass Transition," ASME J. Turbomach., **119**(3), pp. 405–411.
[21] Lardeau, S., and Leschziner, M. A., 2006, "Modelling of Wake-Induced Transition in Low-Pressure Turbine Cascades," AIAA J., **44**(8), pp. 1854–1865.
[22] Pacciani, R., Marconcini, M., Fadai-Ghotbi, A., Lardeau, S., and Leschziner, M. A., 2011, "Calculation of High-Lift Cascades in Low Pressure Turbine Conditions Using a Three-Equation Model," ASME J. Turbomach., **133**(3), p. 031016.
[23] Pacciani, R., Marconcini, M., Arnone, A., and Bertini, F., 2012, "URANS Analysis of Wake-Induced Effects in High-Lift, Low Reynolds Number Cascade Flows," ASME Paper No. GT2012-69479.
[24] Arnone, A., Liou, M. S., and Povinelli, L. A., 1992, "Navier–Stokes Solution of Transonic Cascade Flow Using Non–Periodic C–Type Grids," J. Propul. Power, **8**(2), pp. 410–417.
[25] Arnone, A., and Pacciani, R., 1996, "Rotor-Stator Interaction Analysis Using the Navier–Stokes Equations and a Multigrid Method," ASME J. Turbomach., **118**(4), pp. 679–689.
[26] Jameson, A., 1991, "Time Dependent Calculations Using Multigrid With Applications to Unsteady Flows Past Airfoils and Wings," AIAA Paper No. 91-1596.
[27] Rumsey, C. L., Thacker, W. D., Gatsky, T. B., and Grosch, C. E., 2005, "Analysis of Transition-Sensitized Turbulent Equation," AIAA Paper No. 2005-0523.
[28] Wilcox, D. C., 1998, *Turbulence Modeling for CFD*, 2 edition, DCW Ind. Inc., La Canada, CA.
[29] Lardeau, S., Li, N., and Leschziner, M. A., 2007, "Large Eddy Simulations of Transitional Boundary Layers at High Free-Stream Turbulence Intensity and Implications for RANS Modeling," ASME J. Turbomach., **129**(2), pp. 311–317.
[30] Wissink, J. G., and Rodi, W., 2006, "Direct Numerical Simulations of Transitional Flow in Turbomachinery," ASME J. Turbomach., **128**(4), pp. 668–678.
[31] Hatman, A., and Wang, T., 1999, "A Prediction Model for Separated-Flow Transition," ASME J. Turbomach., **121**(3), pp. 594–602.
[32] Hoheisel, H., 1990, "Test Case E/CA-6, Subsonic Turbine Cascade T106, Test Cases for Computation of Internal Flows in Aero Engine Components," AGARD-AR-275.
[33] Pacciani, R., Marconcini, M., Arnone, A., and Bertini, F., 2011, "An Assessment of the Laminar Kinetic Energy Concept for the Prediction of High-Lift, Low-Reynolds Number Cascade Flows," Proc. IMechE A: J. Power Energy, **225**(7), pp. 995–1003.
[34] Michálek, J., Monaldi, M., and Arts, T., 2012, "Aerodynamic Performance of a Very High Lift Low Pressure Turbine Airfoil (T106C) at Low Reynolds and High Mach Number With Effect of Free Stream Turbulence Intensity," ASME J. Turbomach., **134**(6), p. 061009.
[35] Himmel, C., and Hodson, H., 2009, "Modifying Ultra-High Lift Low Pressure Turbine Blades for Low Reynolds Number Applications," 12 ISUAAAT, London, UK, September 1–4, Paper No. I12-S7-3.
[36] Lodefier, K., and Dick, E., 2006, "Modelling of Unsteady Transition in Low-Pressure Turbine Blade Flows With Two Dynamic Intermittency Equations," Flow Turbul. Combust., **76**, pp. 103–132.